Universiteit Antwerpen

This item is the archived peer-reviewed author-version of:

Self-organization of highly symmetric nanoassemblies : a matter of competition

Reference:

Galván-Moya Jesus E., Altantzis Thomas, Nelissen Kwinten, Peeters François, Grzelczak Marek, Liz-Marán Luis M., Bals Sara, van Tendeloo Gustaaf.- Self-organization of highly symmetric nanoassemblies : a matter of competition
ACS nano - ISSN 1936-0851 - 8:4(2014), p. 3869-3875
DOI: http://dx.doi.org/doi:10.1021/nn500715d
Handle: http://hdl.handle.net/10067/1169550151162165141

uantwerpen.be

Institutional repository IRUA

The Institutional Repository IRUA is a subset of the Academic bibliography. As of 1991 the UA library produces an academic bibliography for the University of Antwerp (UA). IRUA contains scientific publications of UA researchers. If allowed the fulltext of the publications are made available.

This item is the archived peer-reviewed author-version of:

Title: Self-organization of highly symmetric nanoassemblies : a matter of competition

Authors: Galván-Moya Jesus E., Altantzis Thomas, Nelissen Kwinten, Peeters François, Grzelczak Marek, Liz-Marán Luis M., Bals Sara, van Tendeloo Gustaaf.

In:ACS nano (2014)

To refer to or to cite this work, please use the citation to the published version:

Galván-Moya Jesus E., Altantzis Thomas, Nelissen Kwinten, Peeters François, Grzelczak Marek, et al. - *Self-organization of highly symmetric nanoassemblies : a matter of competition* - In: ACS nano 8:4(2014), p. 3869-3875

http://dx.doi.org/doi:10.1021/nn500715d

Self-Organisation of Highly Symmetric Nanoassemblies: A Matter of Competition

Jesus E. Galván-Moya[†#], Thomas Altantzis[‡#], Kwinten Nelissen[†], Francois M. Peeters[†], Marek Grzelczak[§,‖], Luis M. Liz-Marzán[§,‖], Sara Bals[‡]*, Gustaaf Van Tendeloo[‡]

[†]CMT, University of Antwerp, Groenenborgerlaan 171, B-2020 Antwerp, Belgium

[‡]EMAT, University of Antwerp, Groenenborgerlaan 171, B-2020 Antwerp, Belgium

[§]Bionanoplasmonics Laboratory, CIC biomaGUNE, Paseo de Miramón 182, 20009 Donostia-San Sebastián, Spain

[‖]Ikerbasque, Basque Foundation for Science, 48011 Bilbao, Spain

AUTHOR INFORMATION

 # Author contribution

J.E.G-M and T.A. equally contributed to this work.

*** Corresponding author**

Email: sara.bals@uantwerpen.be

The authors declare no competing financial interest

ASSOCIATED CONTENT

Supporting information

Details concerning synthesis and structural analysis, extended theoretical analysis and material dependence explanation. This material is available free of charge *via* the internet at http:// pubs.acs.org.

ABSTRACT

The properties and applications of metallic nanoparticles are inseparably connected not only to their detailed morphology and composition, but also to their structural configuration and mutual interactions. As a result, the assemblies often have superior properties as compared to individual nanoparticles. Although it has been reported that nanoparticles can form highly symmetric clusters, if the configuration can be predicted as a function of the synthesis parameters, more targeted and accurate synthesis will be possible. We present here a theoretical model that accurately predicts the structure and configuration of self-assembled gold nanoclusters. The validity of the model is verified using quantitative experimental data extracted from electron tomography 3D reconstructions of different assemblies. The present theoretical model is generic and can in principle be used for different types of nanoparticles, providing a very wide window of potential applications.

Graphical Table of Contents

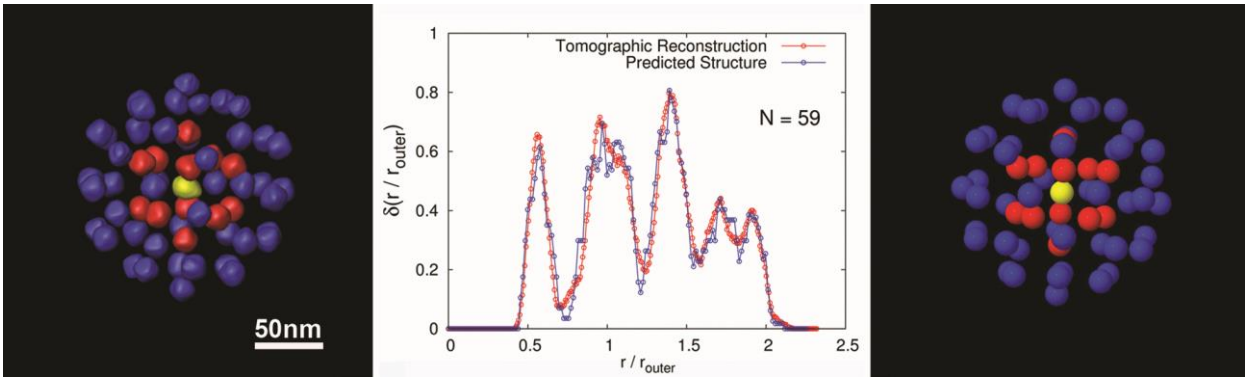

KEYWORDS: Electron tomography, self-assembly, Monte Carlo simulations, pairwise interaction, gold nanoparticles.

Assemblies of nanoparticles in two and three dimensions have gained increasing interest because of their multiple applications[1-5] and improved properties, compared to those of their building blocks.[6-10] By varying experimental parameters, such as the size and shape of the individual particles or the nature and length of the capping ligands, different nanostructures with unique configurations can be obtained. However, the complex mechanism and interplay of the forces and processes leading to a given assembly is often poorly understood and in some cases only empirically found. Having access to such information would enable researchers to predict the stacking of the individual nanoparticles into a specific configuration as a function of the experimental parameters. In this manner, the synthesis of nanoassemblies with tailored properties for specific applications would become much more accurate and efficient. In this work, we demonstrate a thorough understanding of the formation of symmetrical 3D nanoassemblies by combining a state-of-the-art structural analysis with modern computational techniques.

Transmission Electron Microscopy (TEM) is an ideal technique to investigate materials at the (sub)nanometer scale and has therefore been widely used in the study of nanomaterials. In order to understand the connection between structure and properties of these materials, the combination of TEM and theoretical calculations is very powerful.[11-13] However, it is important to realize that TEM images only correspond to a two-dimensional (2D) projection of a three-dimensional (3D) object. In order to gain the necessary structural information concerning the 3D nanoassemblies, 3D TEM, so-called electron tomography, has to be performed.[14-16] Recently, this technique has proven its power in the investigation of 3D nanoassemblies, especially when quantitative data, such as particle diameters or positions, are required.[1,16] 2D self-assembled systems have been theoretically studied in depth during the last decade,[17-25] and the transition between 2D and 3D assemblies has been recently investigated.[22] However, these studies are mainly based on phenomenological models,[1,11,26-29]

but do not yield insight concerning the underlying physical processes involved during the formation of the 3D assemblies.

In the present work, we combined state-of-the-art electron tomography results with a new theoretical model, which is easy to implement and moreover, which provides a thorough understanding of the formation of 3D assemblies from the aggregation of gold nanoparticle building blocks. In the selected example shown in Figure 1, gold nanospheres grafted with polystyrene chains form clusters in solution upon increasing the solvent dielectric constant, where L stands for the polymer chain length, D for the particle diameter and

$$\gamma = \left(1 + \frac{2L}{D}\right)^3 \quad (1)$$

is the ratio of the total volume taken by the particle and the polymer and the volume of the Au particle, which is thus a material independent quantity. This was interpreted as an interplay between van der Waals and hydrophobic attraction and steric repulsion forces. The model we propose here is more general, in the sense that it is based on the competition between a long-range attractive and a short-range repulsive force for each pair of particles. This is explained as an effective interaction between particles, which in the present study will be taken as isotropic, assuming that all nanoparticles are identical and spherical, which is reasonable in the case of the experiments considered here. The combination of electron tomography and the new theoretical model enables us to predict the 3D configuration of the obtained Au nanoassemblies with high accuracy. It is however important to point out that, because of the generality of the model, our approach can be applied to a wide variety of nanoparticle assemblies.

RESULTS AND DISCUSSION

Using electron tomography, the 3D configurations were determined for several assemblies obtained using different synthesis parameters. The most relevant parameters correspond to the diameter of the individual nanoparticles (D) and the polymer chain length (L). The experimental results are presented in Figure 1; they show essentially two different kinds of configurations. For assemblies containing particles with a relatively small diameter grafted with polymers of short chain length (L) a dense packed configuration was found (Figure 1 a-c). However, in the case of longer polymer lengths, shell like structures can be identified (Figure 1 d-i). Strikingly, some of the 3D reconstructions, such as the example presented in Figure 1d yield a highly symmetric and regular 3D stacking of the individual nanoparticles. In Figure 1g, an icosahedron is clearly observed, but also other types of polyhedra were found. It should be noted that for large and more dense packed assemblies, such as the example in Figure 1f, regular stackings were not observed, but the arrangement was closer to spherical symmetry. For certain configurations however, some shells appear to be incomplete, *i.e.* particles are missing. In order to obtain a thorough understanding of the formation of such assemblies, the electron tomography results were compared with computer simulations.

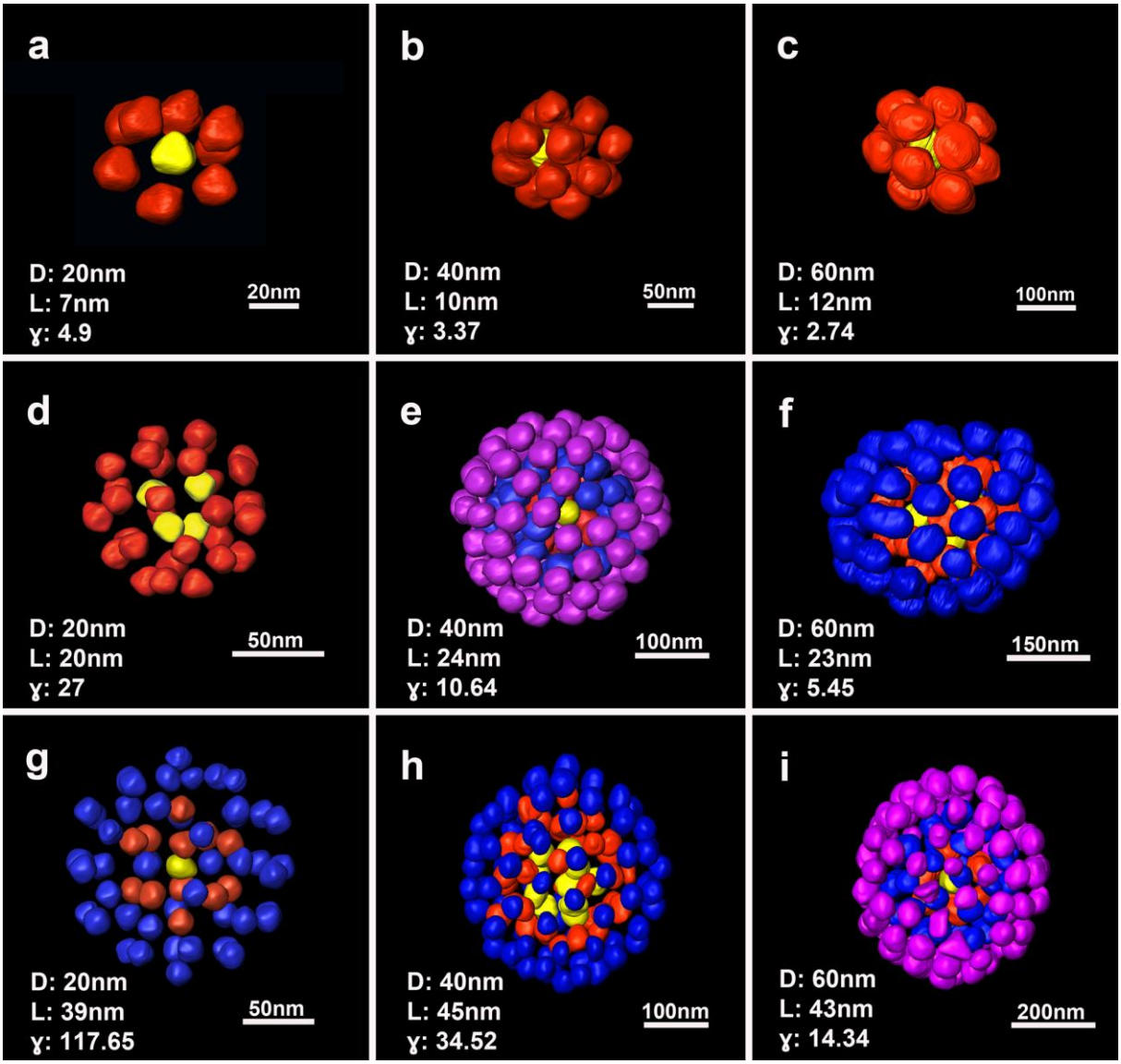

Figure 1. 3D representation of reconstructed assemblies from experimental 2D TEM images at various angles. In each image, the synthesis parameters (D and L) and the value of γ for each configuration are given. Different colors refer to the different shells in the assemblies.

The inter-particle distances in such self-organized systems have been explained theoretically, showing that the interaction between particles is complex and involves many variables.[1,29] Although the model proposed in Reference 1 may very well predict inter-particle distances, it turns out that the 3D configuration of the assemblies can not be obtained. The reason is that in the model of Reference 1, the van der Waals interaction is only correctly described in the limit of close-approach and overestimates the strength of the long-range

interaction. Here, we propose a potential that is based on a generalized Morse inter-particle interaction:

$$E = \sum_{i=1}^{N} \sum_{j>i}^{N} \left(A \exp(-\alpha r_{ij}) - \tilde{B} \exp(-\tilde{\beta} r_{ij}) \right). \quad (2)$$

In this expression A($\tilde{B}$) and α ($\tilde{\beta}$) are real numbers that modulate the strength and the screening of the repulsion (attraction) between particles, N is the number of particles in the assembly, and r_{ij} represents the distance between the centers of the i-th and the j-th particles in the self-assembled system. A similar interaction was used previously to describe the structure of 2D self-organized colloidal systems.[30] For a given temperature T, Equation (2) can be written in dimensionless form as follows:

$$E = \sum_{i=1}^{N} \sum_{j>i}^{N} \left(\exp(-r_{ij}) - B \exp(-\beta r_{ij}) \right), \quad (3)$$

where $\beta = \tilde{\beta} / \alpha$, while the energy and the distances are given in units of $E_0 = AK_BT$ and $r_0 = \alpha \tilde{r}_0$, respectively. The average distance between concentric shells in the assembly is given by $\tilde{r}_0$, which is defined as the characteristic length of the system (see Supporting Information for details). Equation (3) represents a two-parameter model which enables one to tune the strength and the range of the attraction in a flexible manner.

The advantage of this potential is that, in the inter-particle distance range near its minimum, it can be mapped on the potential of Reference 1, from which experimental synthesis conditions can be extracted. Once this relationship has been established and the theoretical parameters have been linked to the synthesis conditions, the procedure can be reversed and thus, starting from experimental synthesis conditions the final configuration can be predicted.

The ground state configuration is obtained by Monte Carlo (MC) simulations supplemented with the Newton optimization method. This approach has been successfully

used in previous works.[17,31,32] As a first result, irrespective of the values of B and β, we notice that the model is translational and rotational invariant. Due to the isotropic inter-particle interaction, highly symmetric structures were found, in agreement with our electron tomography results. Based on numerical simulations, a good agreement with the experimental results has been found with $\beta = 0.5$, for all samples investigated. This implies a relative short-range attraction between the particles. The parameter B can be used as an adjustable parameter that determines the packing density. A detailed discussion on the relation between the present model and the synthesis parameters can be found in the Supporting Information.

In order to correlate the experimental data with the theoretical calculations, we introduce the mass density inside the shell defined by the ends of the polymer chains surrounding each gold nanoparticle, which is given by $\rho = \rho_c / \gamma$, where ρ_c is the density of Au. Experimentally, we found that for $\gamma >> 1$, *i.e.* long polymer chain lengths with respect to the particle size, the assembly formed by the nanoparticles is highly spherical symmetric (see Figure 1). As can be seen from Equation (3), the parameter B is a measure for the attraction between each pair of particles. For smaller values of γ, and taking into account that the polymer chain lengths are comparable to the particle size, the distance between Au nanoparticles will be small and consequently deviations from the non-spherical geometry of the nanoparticles will become important in the self-assembly process, which are not taken into account in the present analysis. In this case information about the detailed shape of the nanoparticles is needed in order to construct a non-spherical symmetric inter-particle interaction, which is beyond the scope of the present work. As an example, we model three different clusters, which correspond to Figures 1 d, g, h. For the largest γ-values, as those listed in Table 1, the best fit with the tomographic reconstruction was found with $B = 0.65$.

Sample	D(nm)	L(nm)	γ	N	n	Shell-like Configuration	
						Tomographic Reconstruction	Theoretical Prediction
A	20	20	27.00	33	2	(4, 29)	(4, 29)
B	20	39	117.65	59	3	(1, 12, 46)	(1, 12, 46)
C	40	45	34.52	132	3	(11, 37, 84)	(10, 37, 85)

Table 1. Experimental sample parameters: D is the diameter of the Au particles and L is the length of the polymer chains surrounding them, N is the number of particles and n is the number of shells found in each cluster. The number of particles per shell for the experimental assemblies and for the theoretical model with B=0.65 are displayed in the two rightmost columns.

The best agreement between theory and experiment was achieved for large γ-values, when complete shell structures, *i.e.* without vacancies, are formed experimentally. We therefore focus on the interpretation of the three different assemblies having large γ-values, with the experimental parameters listed in Table 1.

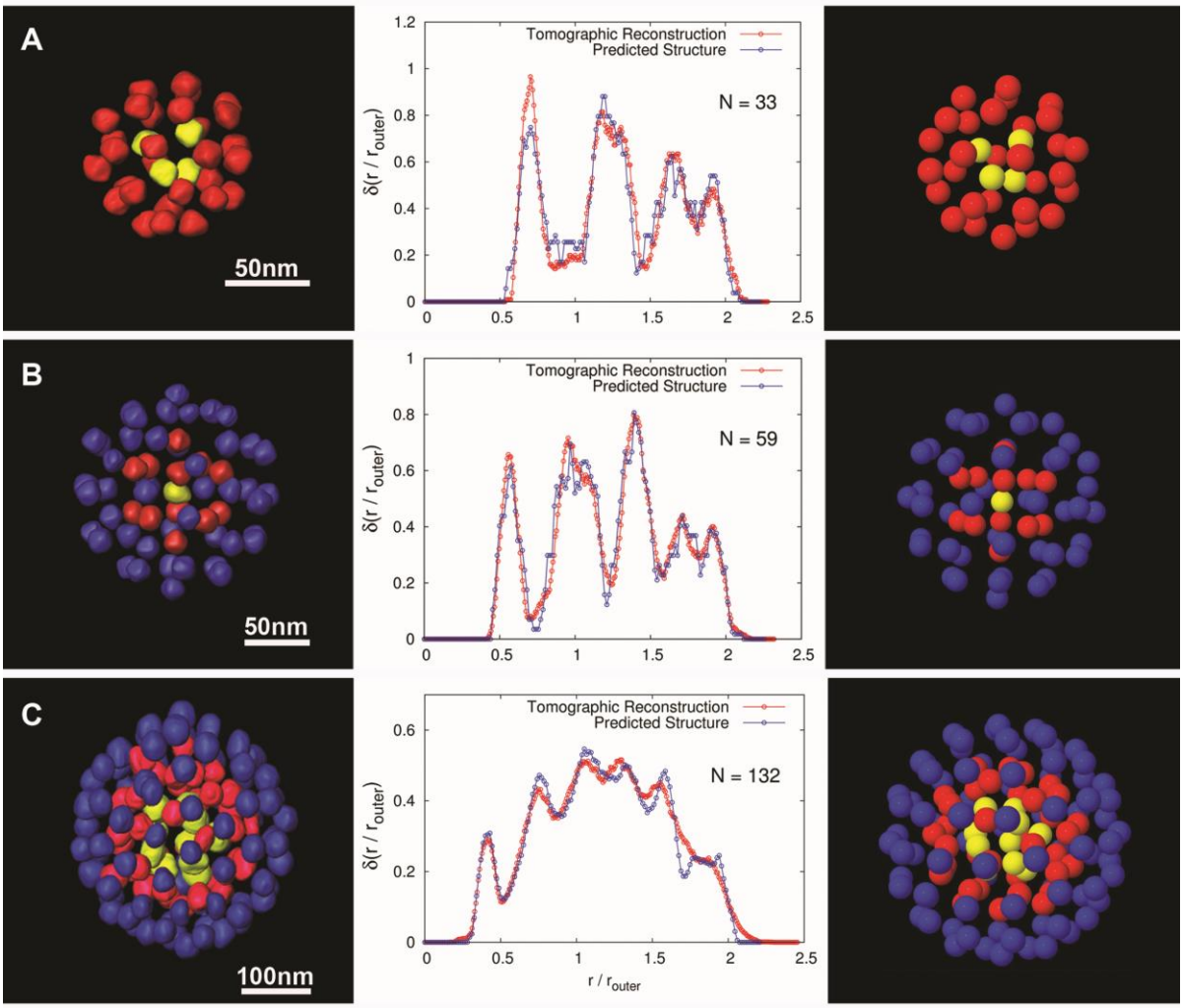

Figure 2. Comparison between configurations obtained from experimental reconstruction (left) and simulations (right) with the parameters listed in Table 1. Particles belonging to different shells are highlighted by different colors. In the central panel, the radial density distribution function is plotted, where we compare the experimental results with the ones obtained from theory.

Figure 2 demonstrates the excellent agreement between the theoretical predictions and the experimental configurations obtained by tomographic reconstruction. The comparison between experiment and simulations is based on the number of particles per shell (rightmost columns of Table 1). It can be seen that the simulations predict with high precision the particle positions for small and intermediate cluster sizes ($N = 33, 59$), whereas a small discrepancy of only one particle between the inner and the outer shell is found for the largest

one ($N = 132$). To further confirm the agreement we plotted the radial density distribution of the assemblies ($\delta(r)$) as a function of the interparticle distance, which for this figure is scaled by the radius of the outer shell (r_{outer}). This function is defined as the probability to find two particles separated by a distance r, and is closely related to the radial distribution function, which is used to describe the structure of the assemblies for larger systems.[13]

Based on the use of $\delta(r)$, a comparison is presented in the central panel of Figure 2. For the experimental data we used the coordinates of the center of mass of all nanoparticles in each assembly, as they were extracted from the tomographic reconstructions. The radial densities show very good agreement not only in the number of peaks, which is intrinsically related to the shell-like structure, but also with respect to the location and height of the peaks.

Also from the simulation results it is clear that the particles at the inner shells of the assemblies preferably sit in highly symmetric polyhedral structures. For example, the third column of Figure 2 confirms that the inner shell of sample A is formed by a regular tetrahedron, and the second shell of sample B forms a regular icosahedron (see Supporting Information). These are just few examples of regular structures that can be found. It must be noted that also octahedra and different elongated bipyramidal structures are predicted by our model, to form the inner shell configuration of assemblies with different numbers of particles. This finding is in contrast to Lennard-Jones assemblies, which were recently found to organize in planar configurations.[11]

Simulations carried out for assemblies with an increasing number of particles enabled us to describe the self-assembly process as follows: initially, for a small number of particles ($N < 12$), all particles are arranged in a single shell, forming configurations such as antiprisms and bipyramids but with regular polyhedra (tetrahedron, octahedron and icosahedron) being dominant. Next, as the number of particles increases, the potential energy minimization procedure results in a rearrangement of the particles generating new shells of

particles leading to an increase of the radius of the outer shell and an increase of the inter-shell distances. After increasing the number of particles further it becomes energetically more favorable to occupy the next inwards located shell due to the high surface tension of the former shell. This process is repeated shell after shell till the most inner shell reaches a critical size leading to a void at the center of the assembly. After a further particle addition, this void is occupied by an additional particle, resulting in the formation of a new shell. Such assembly configurations can be grouped in Mendeleev-like tables as function of the number of particles, an example is given in the supporting information.

In order to illustrate the physics behind the 3D assembly process, we show in Figure 3 the phase diagram of the ground state configurations for a system with $N = 59$ particles as a function of the parameters in our model. In this figure, the different letters represent different configurations of the system, which are given at the right side of the figure by the number of particles in each shell. The thick solid arrow indicates the direction of increasing packing fraction. Please note that the best fit with the present experiment was obtained for $B = 0.65$ and $\beta = 0.5$. All transitions between different configurations were found to be of first order.

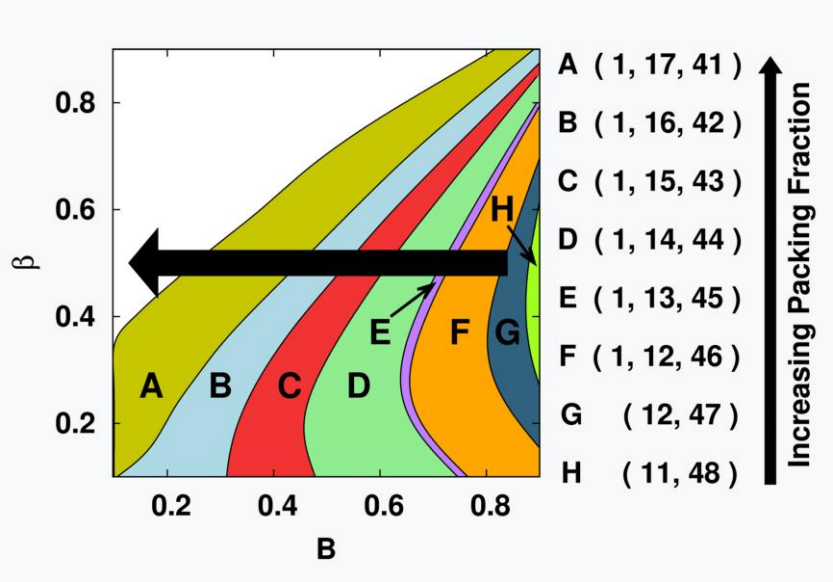

Figure 3. Phase diagram of the ground state configuration of an assembly with $N = 59$ gold nanoparticles, as a function of the theoretical parameters B and β. Different colors represent different configurations as they are labeled alphabetically in the figure. The number of particles per shell for each configuration is indicated in the column on the right side. The thick solid arrow indicates the direction of increasing packing fraction.

Following the configurations as they are alphabetically ordered in Figure 3, one can observe that increasing the attraction (B) leads to the migration of particles from the inner to the outer shells. This is a consequence of the reduction of the inter-particle distance allowing the outer shells to accommodate more particles.

In Figure 3, the configurations at the left of A can no longer be described as shell-like structures; they are structures with planar faces, which is typical for particles interacting through a Lennard-Jones or Morse potential.[11,27] Starting from configuration A and by increasing parameter B, all configurations retain a shell-like structure after going through the following configurations: dense packed configuration → regular triangular configuration (polyhedral configurations) → spherical-like shell configuration. The last transition occurs through a continuous process of shell radius reduction.

Our theoretical approach allows us to explain the formation of the assemblies and to correctly predict their 3D configuration for the considered synthesis parameters of our samples. The observed structures result from the tendency of the system to form a close packed configuration, as obtained for small values of B, as well as from the formation of a shell-like structure due to strong attraction. The stronger the attraction, the more particles can be packed on a specific shell, and the more shell-like the final structure will be. This phenomenon is closely related to the surface tension, where the attraction between molecules or atoms results in the minimization of the surface formed by the particles on the outer shell. This competition results, in the case of strong attraction, in a sequential formation of regular polyhedra. Although shell-like structures are expected to form for large γ-values, experimental evidence showed that this is the case even in the region $27 \leq \gamma \leq 117$. Experimentally, close packed configurations are expected for nanoparticles with a weak attraction, while shell-like structures are expected to be formed for nanoparticles with a strong attraction.

In the formation process previously described, we found that the attraction between particles is of relative short-range character ($\beta = 0.5$). This allowed us to obtain an optimal agreement between theory and experiment (Figure 2), showing that the screening of the attraction is not affected by either the particle size or the polymer length. The relation between synthesis parameters and the model parameter B is obtained by fitting the potential presented in Reference 1 around the local minimum with our model (Equation (3)). In Figure 4 this relation is given for different values of particle size (D) and polymer length (L). All synthesis parameters are listed in the supporting information.

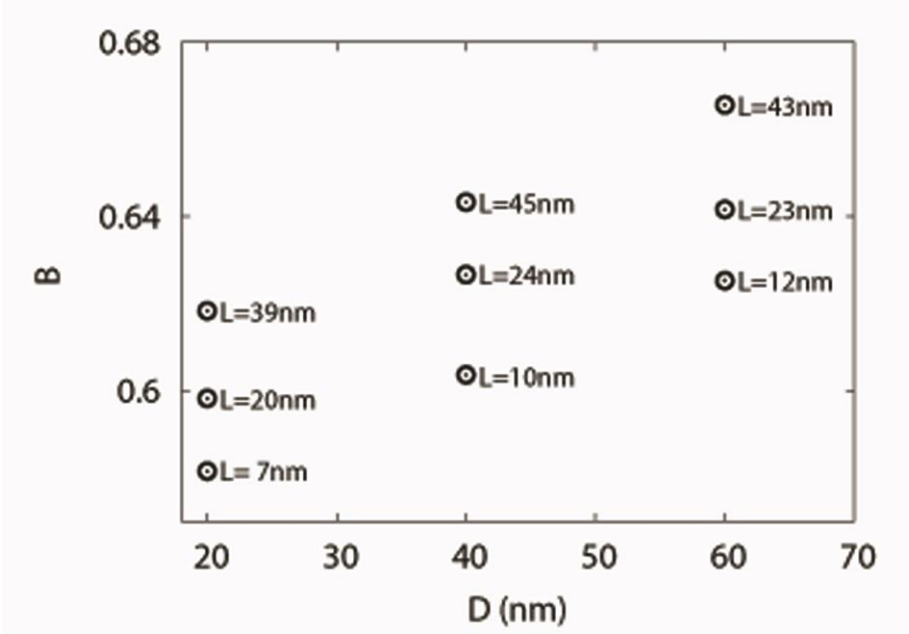

Figure 4. Theoretical parameter (B) plotted as a function of the particle diameter (D) for different values of the polymer chain length (L). These points have been calculated by adjusting the energy curve proposed in Reference 1 through Equation (3) for $\beta = 0.5$. A complete list of the synthesis parameters considered in the present calculation is shown in the supporting information.

From Figure 4 one can see that the value of B is proportional to both particle size and polymer chain length. From these results, one can conclude that the attraction between particles increases with the polymer length (which may be related to hydrophobic forces), but that the increment becomes less significant for smaller particle sizes (where van der Waals forces are weaker). Figure 4 reveals that the values of B are in the interval [0.58, 0.67] (see supporting information), which confirms the validity of the present model where the theoretical structures correspond to B=0.65 (see Figure 2). These results indicate that by increasing the polymer chain length the strength of the attraction between particles increases, resulting in a reduced packing fraction and a more symmetrical configuration.

CONCLUSIONS

Nanoparticles in the 10-100 nm range tend to self-organize into three dimensional clusters. This self-organization process of spherical nanoparticles into spherical assemblies was investigated, both experimentally and theoretically, using a pairwise interaction; Au nanoparticle assemblies formed by inducing hydrophobic forces were chosen as a case study. We proposed a new model, based on a simple competition between attractive and repulsive interactions which we were able to relate with the experimental synthesis parameters. The excellent agreement between the experimentally observed and the theoretically predicted configurations provides us with the opportunity to understand the physics behind cluster formation. For the synthesis parameters used, we can explain the particular cluster formation and correctly predict their 3D configuration. The final structures result from the tendency of the system to form a close packed configuration and the formation of a shell-like structure induced by strong attraction. The stronger the attraction, the more particles can be packed on a specific shell, and the more shell-like the final structure will be. This is closely related to the phenomenon of surface tension where the attraction between molecules or atoms results in the minimization of the outer surface area. This competition results, in the case of strong attraction, in a sequential formation of regular polyhedra.

Our theoretical model may enable one to guide the synthesis of novel 3D assemblies in a controlled and efficient manner, which will be of importance for different scientific applications where specific 3D arrangements of nanoparticles are required, such as metamaterials or nanoparticle assemblies with optimized hot spot density.

Acknoledgments

This work was supported by the Flemish Science Foundation (FWO-Vl) and the Methusalem programme of the Flemish government. Computational resources were provided by HPC infrastructure of the University of Antwerp (CalcUA) a division of the Flemish Supercomputer Center (VSC). The authors acknowledge financial support from European Research Council (ERC Advanced Grant # 24691-COUNTATOMS, ERC Advanced Grant # 267867-PLASMAQUO, ERC Starting Grant # 335078-COLOURATOMS). The authors also appreciate financial support from the European Union under the Seventh Framework Program (Integrated Infrastructure Initiative N. 262348 European Soft Matter Infrastructure, ESMI).

METHODS

Synthesis. Nine batches of gold nanoparticles (18.0 ± 0.5 nm, 40.0 ± 0.9 nm and 61.7 ± 1.5nm), stabilized with polystyrene (Mw = 5.8, 21.5, 53 kg/mol) were prepared according to experimental conditions reported in Reference 1. In a typical assembly experiment, water (0.4 mL) was added to the polystyrene-stabilized gold colloid (1.6 mL, THF) under magnetic stirring. After 10 minutes, a solution of polystyrene-block-polyacrylic acid was added in THF (6 mg/mL, 0.2 mL). Subsequently, the water content was increased up to 35 wt %, followed by increasing the temperature to 70 ºC, which was maintained for 1 h. The final solution was centrifuged twice and dispersed in pure water. As-prepared clusters were used for imaging without further processing.

Structural analysis. Electron microscopy observations were carried out using a FEI Tecnai G2 electron microscope operated at 200 kV. A Fischione tomography holder (model 2020) was used for the acquisition of the tilt series of 2D projection images. All tilt series were acquired in High Angle Annular Dark Field Scanning Transmission Electron Microscopy (HAADF-STEM) mode with an annular range from -74^{o} to +76^{o} and a tilt

increment of 2^{o}. The alignment of the series was performed in Inspect 3D software (FEI). All the reconstructions were performed using the Simultaneous Iterative Reconstruction Technique (SIRT), as implemented in Inspect 3D.

REFERENCES

1. Sánchez-Iglesias, A.; Grzelczak, M.; Altantzis, T.; Goris, B.; Perez-Juste, J.; Bals, S.; Van Tendeloo, G.; Donaldson Jr., S. H.; Chmelka, B. F.; Israelachvili, J. N. *et al.* Hydrophobic Interactions Modulate Self-assembly of Nanoparticles. *ACS Nano* **2012**, *6*, 11059-11065.

2. Grzelczak, M.; Vermant, J.; Furst, E. M.; Liz-Marzán, L. M. Directed Self-Assembly of Nanoparticles. *ACS Nano* **2010**, *4*, 3591-3605.

3. Zhenda, L.; Yadong, Y. Colloidal Nanoparticle Clusters: Functional Materials by Design. *Chem. Soc. Rev.* **2012**, *41*, 6847-6887.

4. Shevchenko, E. V.; Talapin, D. V.; Rogach, A. L.; Kornowski, A.; Haase, M.; Weller, H. Colloidal Synthesis and Self-Assembly of $CoPt_3$ Nanocrystals. *J. Am. Chem. Soc.* **2002**, *124*, 11480-11485.

5. Shevshenko, E. V.; Talapin, D. V.; Kotov, N. A.; O'Brien, S.; Murray, C. B. Structural Diversity in Binary Nanoparticle Superlattices. *Nature* **2006**, *439*, 55-59.

6. Buck, M. R.; Bondi, J. F.; Schaak, R. E. A total-synthesis framework for the construction of high-order colloidal hybrid nanoparticles. *Nat. Chem.* **2012**, 4, 37-44.

7. Yu, W. W.; Chang, E.; Drezek, R.; Colvin, V. L. Water-Soluble Quantum Dots for Biomedical Applications. *Biochemical and Biophysical Research Communications* **2006**, 348, 781-786.

8. Long, N. V.; Chien, N. D.; Hayakawa, T.; Hirata, H.; Lakshminarayana, G.; Nogami, M. The Synthesis and Characterization of Platinum Nanoparticles: A Method of Controlling the Size and Morphology. *Nanotechnology* **2010**, 21 035605.

9. Perez-Juste, J.; Pastoriza-Santos, I.; Liz-Marzan, L. M.; Mulvaney, P. Gold Nanorods: Synthesis, Characterization and Applications. *Coord. Chem. Rev.* **2005**, *249*, 1870-1901.

10. Yi, D. K. ; Selvan, S. T.; Lee, S. S.; Papaefthymiou, G. C.; Kundaliya, D.; Ying, J. Y. Silica-Coated Nanocomposites of Magnetic Nanoparticles and Quantum Dots. *J. Am. Chem. Soc*. **2005**, 127, 4990-4991.

11. Lacava, J.; Born, P.; Kraus, T. Nanoparticle Clusters with Lennard-Jones Geometries. *Nano Lett.* **2012**, 12, 3279-3282.

12. Bals, S.; Van Aert, S.; Romero, P. C.; Lauwaet, K.; Van Bael, J. M.; Schoeters, B.; Partoens, B.; Ycelen, E.; Lievens, P.; Van Tendeloo, G. Atomic Scale Dynamics of Ultrasmall Germanium Clusters. *Nat. Commun.* **2012**, *3*, 1-6.

13. Miao, Y.; Liu, Y.; Hu, L.; Helseth, L. E. Colloidal Clustering of Protein-Coated Microspheres in Evaporating Droplets. *Soft Matter* **2012**, *8*, 2267-2273.

14. Bals, S.; Casavola, M.; Van Huis, M.; Van Aert, S.; Batenburg, K. J.; Van Tendeloo, G.; Vanmaekelergh, D. Three-Dimensional Atomic Imaging of Colloidal Core-Shell Nanocrystals. *Nano Lett.* **2011**, *11*, 3420-3424.

15. Midgley, P. A.; Weyland, M. 3D Electron Microscopy in the Physical Sciences: The Development of Z-Contrast and EFTEM Tomography. *Ultramicroscopy* **2003**, *96*, 413-431.

16. Altantzis, T.; Goris, B.; Sánchez-Iglesias, A.; Grzelczak, M.; Liz-Marzán, L. M.; Bals, S. Quantitative Structure Determination of Large Three-Dimensional Assemblies. *Part. Part. Syst. Charact.* **2013**, *30*, 84-88.

17. Nelissen, K.; Partoens, B.; Peeters, F. M. Bubble, Stripe, and Ring Phases in a Two-Dimensional Cluster with Competing Interactions. *Phys. Rev. E* **2005**, *71*, 066204.

18. Liu, Y. H.; Chen, Z. Y.; Huang, F.; Yu, H. Y.; Wang, L.; Bogaerts, A. Simulation of Disk- and Band-Like Voids in Dusty Plasma Systems. *Phys. Plasmas* **2006**, *13*, 052110.

19. Liu, Y. H.; Chew, L. Y.; Yu, M. Self-Assembly of Complex Structures in a Two-Dimensional System with Competing Interaction Forces. *Phys. Rev. E* **2008**, *78*, 066405.

20. Nelissen, K.; Matilus, A.; Partoens, B.; Kong, M. Peeters, F. M. Spectrum of Classical Two-Dimensional Coulomb Clusters. *Phys. Rev. E* **2006**, *73*, 016607.

21. Schwarzer, D. F.; Kahl, G. Two-Dimensional Systems with Competing Interactions: Microphase Formation *Versus* Liquid-Vapour Phase Separation. *J. Phys.: Condens. Matter* **2010**, *22*, 415103.

22. Choueiri, R. M.; Klinkova, A.; Thérien-Aubin, H.; Rubinstein, M.; Kumacheva, E. Structural Transitions in Nanoparticle Assemblies Governed by Competing Nanoscale Forces. *J. Am. Chem. Soc.* **2013**, *135*, 10262-10265.

23. Yang, W.; Nelissen, K.; Kong, M.; Zeng, Z.; Peeters, F. M. Structure of Binary Colloidal Systems Confined in a Quasi-One-Dimensional Channel. *Phys. Rev. E* **2006**, *79*, 041406.

24. Zhao, H. J.; Misko, V. R.; Peeters, F. M. Analysis of Pattern Formation in Systems with Competing Range Interactions. *New J. Phys.* **2012**, *14*, 063032.

25. Costa Campos, L. Q.; Apolinario, S. W. S.; Löwen, H. Structural Ordering of Trapped Colloids with Competing Interactions. *Phys. Rev. E* **2013**, *88*, 042313

26. Pyykko, P. Structural Properties: Magic Nanoclusters of Gold. *Nat. Nanotechnol.* **2007**, *2*, 273-274.

27. Wu, J.; Cheng, L. Global Minimum Structures and Structural Phase Diagrams of Modified Morse Clusters: $11 \leq N \leq 30$. *J. Chem. Phys.* **2011**, *134*, 194108.

28. Florea, I.; Demortiere, A.; Petit, C.; Bulou, H.; Hirlimann, C.; Ersen, O. 3D Quantitative Analysis of Platinum Nanocrystal Superlattices by Electron Tomography. *ACS Nano* **2012**, *6*, 2574-2581.

29. Min, Y.; Akbulut, M.; Kristiansen, K.; Golan, Y.; Israelachvili, J. The Role of the Interparticle and External Force in Nanoparticle Assembly. *Nat. Mater.* **2008**, *7*, 527.

30. Sear, R. P.; Chung, S. –W.; Markovich, G.; Gelbart, W. M.; Heath, J. R. Spontaneous Patterning of Quantum Dots at the Air-Water Interface. *Phys. Rev. E* **1999**, *59*, R6255-R6258.

31. Schweigert, V. A.; Peeters, F. M. Spectral Properties of Classical Two-Dimensional Clusters. *Phys. Rev. B* **1995**, *51*, 7700-7713.

32. Galván-Moya, J. E.; Nelissen, K.; Peeters, F. M. Structural Transitions in Vertically and Horizontally Coupled Parabolic Channels of Wigner Crystals. *Phys. Rev. B.* **2012**, *86*, 184102.